Genetic background influences the heterogeneous phenotypes driven by the MAFA^{S64F} MODY variant in male mice.

Zachary Loyd[1,*], Dongsoo Lee[1,*], Mallory Maurer[1], Jin-Hua Liu[2], Min Guo[2], Garrett Reynolds[2], Mark A. Magnuson[2] , Jean-Philippe Cartailler[2,3], Roland Stein[2], Jeeyeon Cha[1,2,4,§]

[1]Division of Diabetes, Endocrinology, and Metabolism, Department of Medicine, Vanderbilt University Medical Center, Nashville, TN, USA

[2]Department of Molecular Physiology and Biophysics, Vanderbilt University, Nashville, TN, USA

[3]Creative Data Solutions, Vanderbilt Center for Stem Cell Biology, Vanderbilt University, Nashville, TN, USA

[4]VA Tennessee Valley Healthcare System, Nashville, TN, USA

*Co-first authors

[§]Corresponding author: jeeyeon.cha@vumc.org

ABSTRACT

Pancreatic β-cells require several key factors to appropriately secrete insulin to maintain euglycemia. One such factor is MafA, a transcription factor fundamental to β-cell function. We previously identified that a rare, naturally occurring mutation in MAFA ($MAFA^{S64F}$) predisposes carriers to heterogenous conditions of either adult-onset diabetes or hypoglycemia. Curiously, $MAFA^{S64F}$-associated diabetes is much more prevalent in men while women tend to present with hypoglycemia. A mouse model harboring this mutation (termed $MafA^{S64F/+}$) mimicked the heterogeneous, sex-dependent phenotype: female $MafA^{S64F/+}$ mice were hypoglycemic, while male $MafA^{S64F/+}$ mice were hyperglycemic due to widespread, premature β-cell aging and senescence.

Here we show that genetic background modulates these heterogenous phenotypes: while male $MafA^{S64F/+}$ mice on a mixed background of C57/Bl6J and SJL manifest overt diabetes by 5 weeks of age, $MafA^{S64F/+}$ males on a C57/Bl6J background prevents this pathology. In contrast, female mice on both backgrounds (mixed and C57/Bl6J) similarly show hypoglycemia. We find that C57 $MafA^{S64F/+}$ males show improved insulin secretion, abrogation of β-cell senescence, and an islet MafA phosphorylation profile more similar to $MafA^{WT}$ males. Indeed, the abundance of $MafA^{S64F}$ in C57 $MafA^{S64F/+}$ male islets was reduced compared to those from mixed background mice. Bulk RNAseq of isolated islets revealed differentially expressed genes (DEGs) including those encoding factors critical for insulin production, including Nkx6.2, Glis1, and Onecut1 and production of non-insulin islet hormones such as Cck, Gast, Gcg, and Sst. CUT&RUN mapping of MafA DNA binding sites in mouse β-cells identified putative MafA-targets, and overlay of these CUT&RUN peaks with DEGs of each genetic background identified uniquely affected pathways, such as circadian regulation by $MafA^{S64F}$ in the mixed background. In sum, these data identified heterogeneity in glycemic phenotypes across genetic background as a result of differences in islet $MafA^{S64F}$ abundance and distinct pathways affected in $MafA^{S64F/+}$ β-cells at the intersection of cellular aging and circadian entrainment to modulate diabetes susceptibility.

INTRODUCTION

Pancreatic β-cells require several key factors to appropriately secrete insulin to maintain euglycemia. One such factor is the large V-Maf avian musculoaponeurotic fibrosarcoma transcription factor MafA, a pancreatic β-cell-enriched protein that is essential for activating transcriptional programs to promote β-cell maturation and function. Inducing MafA expression in normally non-glucose-responsive and $MafA^{Low}$ neonatal rat islets increases glucose stimulated insulin secretion (GSIS) (*1*). Moreover, acute introduction of MAFA in mouse and human stem cells directly promotes insulin production and β-cell maturity (*1-3*), highlighting the therapeutic potential of maintaining MAFA levels in β-cells (*4-7*). In contrast, compromised MafA levels reduce mouse (*8-13*) and human (*14, 15*) β-cell activity. Indeed, human *MAFA* expression is reduced in islets recovered from donors with type 1 and type 2 diabetes (*14*).

Pathogenic mutations in MAFA is recognized in maturity-onset diabetes of the young (MODY), a collection of monogenic forms of diabetes predominantly driven by mutations in essential islet-enriched transcription factors (*16*). Heterozygous individuals carrying a mutation in the MAFA transactivation domain substituting the conserved serine at position 64 with a phenylalanine (p.Ser64Phe [S64F]) develop either diabetes mellitus or insulinomatosis, a non-syndromic condition of hyperinsulinemic hypoglycemia caused by multiple insulin-secreting neuroendocrine tumors (*17*). Curiously, $MAFA^{S64F}$-associated diabetes is much more prevalent in men (i.e., 3:1) while women tend to present with hypoglycemia (i.e., 4:1) (*17*). A mouse model harboring this clinically pathogenic mutation in the endogenous *MafA* gene (termed $MafA^{S64F/+}$) on a mixed genetic background mimicked the heterogeneous, sex-dependent phenotypes: female $MafA^{S64F/+}$ mice were hypoglycemic, while male $MafA^{S64F/+}$ mice were hyperglycemic due to widespread, premature β-cell aging and senescence (*18*).

In addition to the influence of biologic sex (*19*), mouse genetic background can impart profound effects on whole body glycemia and insulin secretion (*20*). Here we show that genetic background modulates the heterogenous phenotypes of $MafA^{S64F/+}$ mice: while male $MafA^{S64F/+}$ mice on a mixed background of C57/Bl6J and SJL ("mixed") manifest overt diabetes by 5 weeks of age, mutant males on a C57/Bl6J ("C57") background prevents this pathology. In contrast, female mice on both backgrounds (mixed and C57) similarly show a mild hypoglycemia. We find that C57 $MafA^{S64F/+}$ males show improved insulin secretion, abrogation of β-cell senescence, and an islet MafA phosphorylation profile more similar to $MafA^{WT}$ littermate males and reduced abundance of islet $MafA^{S64F}$ compared to those from mixed background males. RNA sequencing on isolated islets from male mice of mixed and C57 genetic backgrounds revealed differentially

expressed gene (DEGs) in each context. Overlaying DEGs with MafA CUT&RUN peaks in mouse β-cells identified uniquely affected pathways such as the circadian regulation by MafA^{S64F} specifically in the mixed background. In sum, these data identified heterogeneity in glycemic phenotypes across genetic background as a result of differences in abundance of islet MafA^{S64F} and distinct pathways affected in MafA$^{S64F/+}$ β-cells at the intersection of cellular aging and circadian entrainment to modulate diabetes susceptibility.

METHODS

Mice

MafA$^{S64F/+}$ heterozygous mice were originally generated using CRISPR/Cas9 targeting by the University of Michigan Transgenic Core on a mixed SJL and C57BL/6J mouse strain, as previously described (*18*). Mice were backcrossed eight generations with C57BL/6J mouse strain (Jackson Lab) to generate MafA$^{S64F/+}$ mice on the C57 background ("C57"). These C57 MafA$^{S64F/+}$ mice were crossed one time with SJL mice (Taconic) to reproduce a new mixed genetic background strain with largely 50:50 contribution of SJL and C57BL/6J ("Mixed") studied in this report. Proportional contributions of genetic backgrounds were confirmed by MUGA analysis (Transnetyx). Mice of both sexes were used in this study; details can be found in the results section and figure legends. All animal studies were reviewed and approved by the Vanderbilt University Institutional Animal Care and Use Committee. Mice were housed and cared for according to the Vanderbilt Department of Animal Care and the Institutional Animal Care and Use Committee of Animal Welfare Assurance Standards and Guidelines.

Intraperitoneal glucose and testing

Glucose tolerance testing was performed on MafA^{WT} and MafA$^{S64F/+}$ mice (n = 6-16) in the afternoon given an intraperitoneal injection of D-glucose (2 mg/g body weight) prepared in sterile PBS (20% w/v) after a 6-hour fast (i.e. 8AM to 2PM). Insulin tolerance tests were conducted in the afternoon by intraperitoneal injection of 0.5 IU/kg body weight insulin (Novolin, regular human insulin, recombinant DNA origin) into mice (n = 3-5) fasted for 6 hours. Blood glucose was measured using a FreeStyle glucometer (Abbott Diabetes Care) before (0 minutes) and at 15, 30, 60, and 90 minutes following injection. Serum insulin and C-peptide was measured by Ultrasensitive Insulin ELISA (Mercodia) and C-peptide ELISA (Alpco), respectively.

Islet isolation and gene expression quantification

Mouse islets were isolated using collagenase P (Sigma) injected into the pancreatic duct, followed by a Histopaque 1077 (Sigma-Aldrich) gradient. Islets were isolated and handpicked in standard RPMI-1640 medium (Thermo Fisher Scientific) supplemented with 10% FBS, L-glutamine, and penicillin-streptomycin, then frozen down in islet pellets. Islet RNA was then isolated using the RNAqueous Micro Total RNA Isolation Kit (Invitrogen). cDNA was generated using Superscript III reverse transcriptase (Invitrogen) by the oligo(dT) priming method. Real-time PCR assays were performed using the LightCycler FastStart DNA Master PLUS SYBR

Green kit (Roche) and a LightCycler PCR instrument (Roche). The real-time PCR primers are listed in Supplemental Table 1. Gapdh or β-Actin was used to normalize the data. Real-time PCR results were analyzed using the ΔΔCt method (*13*).

Cell culture

Monolayer cultures of MIN-6 cells were grown under conditions described previously (*9*). Transfection with scrambled control, $MAFA^{WT}$ or $MAFA^{S64F}$ constructs of confirmed sequences (*21*) was performed using Lipofectamine 2000 (Invitrogen) (average transfection efficiency 80%). RNA was isolated 4 days posttransfection using the Trizol reagent (Fisher Scientific). cDNA was generated using Superscript III reverse transcriptase (Invitrogen) by the oligo(dT) priming method. Real-time PCR assays were performed using the LightCycler FastStart DNA Master PLUS SYBR Green kit (Roche) and a LightCycler PCR instrument (Roche). The real-time PCR primers are listed in Supplemental Table 1. Gapdh or β-Actin was used to normalize the data. Real-time PCR results were analyzed using the ΔΔCt method.

Immunohistochemical analyses

Mouse pancreata were fixed overnight on ice in 4% paraformaldehyde (Electron Microscopy Services) in PBS, and pancreata were embedded in either Tissue-Plus OCT (Thermo Fisher Scientific) or paraffin wax. Sections of rodent pancreata were cut at 6μm thickness. The paraffin sections were deparaffinized and rehydrated before citrate buffer–based antigen retrieval. Sections were then made permeable by 0.5% Triton treatment for 10 minutes. Following blocking with 0.5% BSA in PBS for 120 minutes, the primary antibodies were applied overnight at 4°C. Species-matched antibodies conjugated with the Cy2, Cy3, or Cy5 fluorophores were used for secondary detection (1:1000; Jackson ImmunoResearch). DAPI was used for nuclear staining (Southern Biotech). Immunofluorescence images were obtained using the Zeiss Axio Imager M2 widefield microscope with ApoTome.

Senescence-associated β-galactosidase (SA-β-gal) staining

Pancreata were snap frozen in O.C.T. and cryosections were prepared at 16μm thickness. SA-β-gal activity staining was performed at pH 6.0 (*18*) (Cell Signaling). To compare the intensity of SA-β-gal staining, sections from different genotypes and ages were processed on the same slide. Staining reactions were developed for 18 hours at 37°C, then quenched by 3x PBS washes (pH 7.4). Slides were then subject to immunostaining for insulin by fixing in 4% paraformaldehyde for 45 minutes, permeabilized with Tris-buffered saline with 0.2% Triton X-

100 for 15 minutes, blocked in 2% normal donkey serum/1% BSA in PBS and incubated overnight with guinea pig anti-insulin (1:500, Fitzgerald 20-IP35) at 4°C. HRP-conjugated secondary antibodies were incubated on slides for 1 hour and detected with the DAB+ chromogen kit (DAKO). After washing, slides were mounted and imaged by brightfield microscopy.

Western blotting

MAFA protein levels were normalized to endogenous β-actin by immunoblotting with anti-MAFA (Cell Signaling Technology, 79737) and anti–β-actin (MilliporeSigma, MAB1501) antibodies. Horseradish peroxidase–conjugated anti-rabbit (31460, Thermo Fisher Scientific) or anti-goat (31402, Thermo Fisher Scientific) secondary antibodies were used at 1:5000. Immunoblots were quantified with ImageJ (NIH).

RNAscope and quantification

$MafA^{WT}$ and $MafA^{S64F/+}$ pancreata from 5-week-old mice were harvested and fixed in 10% neutral buffered formalin for 72 hours. Tissues were embedded in paraffin wax, serially sectioned to 5μm thickness, and air dried for 10-14 days prior to processing. The RNAscope® Multiplex Fluorescent Reagent Kit V2 (ACD) was used following manufacturer's instructions. In short, pancreas sections were incubated at 60°C for one hour, then deparaffinized with xylene, dehydrated, and incubated for an additional 30 minutes. Tissues were treated with hydrogen peroxide for 10 minutes and placed in 1X target retrieval solution (ACD) at 100°C for 15 minutes. Sections were then treated with Protease Plus in ACD HybEZ™ II Oven at 40°C for 30 minutes. Afterward, the sections were incubated with *Cdkn1a* C-1 probe (ACD) at 40°C for 2 hours, followed by 3 amplification steps of 30, 30, and 15 minutes. The probes were visualized with the Opal fluorophores. Co-immunostaining for Insulin protein was performed using guinea pig anti-insulin antibody (Fitzgerald 20-IP35). Cy-2 conjugated secondary antibody and DAPI were incubated on the slides for 1.5 hours. After PBS washes, slides were mounted using Prolong Gold Antifade Mountant (Invitrogen) and imaged on the Leica DMi8 inverted microscope at 40X objective.

RNAscope images were analyzed using QuPath (*22*). Regions of interest (ROI) around islets were defined based on insulin staining positivity. Stardist(*23*) , a deep-learning-based nuclei detection model, was used to detect nuclei and outline the cell via a cell expansion of 2.5 μm. Max entropy or triangle auto-threshold methods and image down-sampling (factor of 2) was used to determine the threshold for each channel with an RNA probe. RNA speckles were

detected using the subcellular detection feature in QuPath with the calculated thresholds. Percentage of β-cells positive for *Cdkn1a* was calculated in QuPath and exported to Prism for statistical analysis.

Bulk RNASeq and analysis of mouse islet cells

Bulk RNA-Seq was performed on MafA$^{S64F/+}$ mouse islets isolated at 5 weeks of age. RNAqueous Micro Total RNA Isolation Kit (Invitrogen) was used to isolate total RNA, and RNA quality was analyzed on an Agilent 2100 Bioanalyzer. Samples with RIN >8 were used for sequencing. The cDNA libraries were constructed, and paired-end sequencing was performed on an Illumina NovaSeq6000 (150-nucleotide reads). The generated FASTQ files were processed and interpreted using the Genialis visual informatics platform (https://www.genialis.com) as described previously(*18*). DESeq2 was used for differential gene expression analyses and statistical comparison, as previously described (*24*). Poorly expressed genes, which have expression count summed over all samples below 10, were filtered out from the differential expression analysis input matrix.

CUT&RUN assay and analysis

CUT&RUN was performed on 500,000 dispersed mouse MIN6 cells per condition using CUTANA ChIC/CUT&RUN protocol v3.1 (Epicypher). Nuclei were extracted with nuclear extraction buffer (20 mM HEPES-KOH [pH 7.9]; 10 mM KCl; 0.1% Triton X-100; 20% glycerol; 1 mM MnCl2; 0.5 mM spermidine; 1uM protease inhibitor; Thermo Fisher Scientific) for 10 minutes on ice and immobilized onto Concanavalin-A beads (EpiCypher). After blocking and washes, samples were incubated with 0.5 µg of rabbit anti-MAFA (Cell Signaling 79737) or rabbit anti-IgG (EpiCypher 13-0042) antibodies overnight at 4°C. pAG-MNase (EpiCypher) was added to nuclei (1:20) and incubated at room temperature for 10 minutes. Targeted chromatin digestion was induced by adding 100 mM $CaCl_2$ and nutating for 2 hours at 4°C. DNA fragments were purified using the CUTANA ChIC/CUT&RUN kit, according to the manufacturer's instructions. DNA was resuspended in 0.1M~ Tris-EDTA buffer solution and used for library preparation with the CUTANA CUT&RUN Library Prep Kit (EpiCypher, 14-1001), according to the v1 manual. Libraries were sequenced as PE150 reads on the NovaSeq platform. All libraries had > 15 million reads. and were processed using the nf-core/cutandrun workflow, v3.1 (*25*). The pipeline performs adapter trimming, alignment to the GRCm38 reference genome, filtering against the mm10 blacklist regions, spike-in normalization, and peak calling using MACS2. The workflow also generates IGV sessions and all track data, which allows for interactive

visualization and exploration. Quality was confirmed by fragment length distribution and fingerprint plots. Nearest gene analysis was performed with peakScout (*26*). Coverage plots were created using ggcoverage (*27*).

Statistical Analysis. Data are expressed as the mean ± SEM. Statistical analysis was performed using GraphPad Prism 9.5.0 (GraphPad Software Inc.). The differences between groups were analyzed by unpaired 2-tailed Student's t test or 2-way ANOVA, as indicated. Differences were considered to be statistically significant at $P < 0.05$.

RESULTS

Glucose tolerance is largely unaffected in MafA$^{S64F/+}$ males on a C57 background, while those on a mixed background manifest frank diabetes and impaired insulin secretion.

We previously identified heterogenous outcomes in response to the MafA^{S64F} variant in mice of a mixed genetic background (C57/Bl6J and SJL) (*18*). Mutant mice of both biological sexes showed improved glucose tolerance at birth, then diverged in phenotype beginning at 5 weeks of age: impaired glucose tolerance was demonstrated in MafA$^{S64F/+}$ males while MafA$^{S64F/+}$ females showed persistently mild hypoglycemia. We backcrossed this mouse line 8 generations to a near-pure C57/Bl6J (C57) genetic background. Strikingly, dysglycemia of male MafA$^{S64F/+}$ mice was prevented (**Fig. 1A**). We decided to cross this C57 MafA$^{S64F/+}$ line one generation with SJL mice (Taconic) to produce a controlled mixed genetic background (i.e. 50% SJL and 50% C57/Bl6J) and recovered the frank dysglycemia in the MafA$^{S64F/+}$ males (**Fig. 1B**). Male dysglycemia in this mixed background was associated with impaired insulin and C-peptide secretion (**Fig. 1C-D**), compared to intact C-peptide secretion in the C57 MafA$^{S64F/+}$ males (**Fig. 1E**). Interestingly, the hypoglycemia phenotype of MafA$^{S64F/+}$ females remained consistent between the genetic backgrounds (**Supp Fig. 1A-B**), with either intact (mixed background) or improved (C57 background) in vivo insulin and/or C-peptide secretion (**Supp Fig. 1C-E**).

We previously reported that MafA$^{S64F/+}$ males show transient hypoglycemia preceding impaired glucose tolerance at 5 weeks of age (*18*). We measured the random glucose levels of 2-3 week old pups on the mixed background and identified that we again see relative hypoglycemia preceding dysglycemia in the male mutant mice, similar to the female mutant mice (**Supp Fig. 2A**) (*18*). We recognized that the time of phenotype onset between 4 and 5 weeks of age coincided with weaning and a shift in dietary intake from nursing to chow pellets. Thus we performed an extended wean protocol to evaluate glycemia of these mice while nursing. Even so, we found that male mutant mice showed elevated random glucose levels compared to their wild type (WT) littermates (**Supp Fig. 2B**), demonstrating the dominant effects of the mutation on glycemia over dietary change. We also found that weight gain as a proxy of overall health was not impacted by the mutation in either genetic background (**Supp Fig. 2C-D**), and peripheral insulin sensitivity was largely intact in all groups (**Supp Fig. 2E**). These results demonstrate heterogeneous impact of the MafA^{S64F} variant across biologic sex and genetic backgrounds, and that these effects are primarily mediated at the level of the pancreatic islet.

Islet endocrine populations are largely unchanged, however, expression of critical islet factors and known MafA targets are altered in MafA$^{S64F/+}$ islets despite MafA^{S64F} binding to the *Insulin* enhancer being similar to MafA^{WT}.

Next, we evaluated the integrity of the pancreatic islets of these mutant male mice across genetic backgrounds. We reported that islets of mutant MafA$^{S64F/+}$ mice were smaller in both males and females across backgrounds, consistent with the reduced β-cell mass seen previously (*18*). We find that the distribution and proportions of insulin-producing β-cells, glucagon-producing α-cells, and somatostatin-producing δ-cells appeared largely similar between groups (**Fig. 2A-B**). Expression of islet-enriched transcription factor Pdx1 was downregulated in MafA$^{S64F/+}$ males both genetic backgrounds, however, this trend was more significant in the mixed background (**Fig. 2C**). As MafA is a transcription factor, we also assessed the expression of known downstream targets, such as Ins1, Ins2, Glp1r, and Gck. These targets were downregulated in MafA$^{S64F/+}$ males of both genetic backgrounds, with the trend being more significant in the mixed background (**Fig. 2D**). Gel shift assay for the *Insulin1* enhancer was performed to evaluate whether binding capacity of the MafA^{S64F} protein to target genes to account for the reduced expression of target genes. However, the binding ability of MafA^{S64F} was similar to the MafA^{WT} protein (**Fig. 2E**). These results suggest similar responses to MafA^{S64F} across backgrounds, with more significant changes in the mixed background.

MafA status is more preserved in C57 MafA$^{S64F/+}$ male islets compared to those from mixed MafA$^{S64F/+}$ males.

To better understand the graded differences in the glycemic phenotype and target gene expression of male MafA$^{S64F/+}$ males, we evaluated the status of islet MafA across genetic backgrounds. MafA is an islet-enriched transcription factor, and its expression is essential for β-cell functional maturity (*1, 28*). It is highly sensitive to cellular stress (*29*) and downregulated in the islets of donors with diabetes (*14*). We previously showed that MafA^{S64F} impairs the normal phosphorylation of this protein to produce an unusually stable protein in vitro (*17*), and transcript levels of MafA are downregulated in vivo through autoregulation (*18*). Protein levels are transiently elevated then downregulated in vivo (*18*), suggesting differences in its in vivo regulation. Here we find that MafA is indeed downregulated at the transcript and protein levels in islets isolated from MafA^{S64F} males the mixed background as we had seen before (**Fig. 3A-B**)

(*18*). Interestingly, we find intact MafA transcript and protein in islets of the MafA$^{S64F/+}$ males the C57 background (**Fig. 3C-D**).

As these are heterozygous mice, we questioned whether the proportions of wild-type (i.e. fully phosphorylated) and MafA^{S64F} (i.e. under-phosphorylated) proteins were differentially produced between the genetic backgrounds. Immunoblotting for MafA on isolated primary islets showed an increased presence of phosphorylated MafA species in the C57 background, compared to a predominant underphosphorylated band in the mixed background (**Fig. 3E**). Quantification of the bands confirmed the predominance of the underphosphorylated MafA species in the mixed background compared to the C57 background, which showed relatively equal proportions (**Fig. 3F**). These results link the differences in the glycemic phenotypes and target gene expression between genetic backgrounds with differential islet MafA^{S64F} abundance and proportions of phosphorylated to under-phosphorylated islet MafA species.

Islet senescence is abrogated in male C57 MafA$^{S64F/+}$ islets.

Accelerated islet senescence is a feature of islets from T1D and T2D donors, which can be recapitulated in mouse models of diabetes such as insulin resistant models (*30*), the NOD model (*31*), and in MAFA^{S64F} MODY (*18*). As we reported previously, accelerated cellular aging of islets was dominant in MafA^{S64F} males in mixed background with islet enrichment of senescence associated-β-galactosidase (SA-β-gal) staining and expression of known senescence markers (**Fig. 4A**). Interestingly, these changes were not evident in the MafA$^{S64F/+}$ male islets from a C57 background (**Fig. 4B**). In particular, the *Cdkn1a* encoding p21, a driver of cell cycle arrest and implicated as a principal driver of β-cell senescence (*32*), was enriched in MafA$^{S64F/+}$ males on a mixed, but not C57, background (**Fig. 4C**). Moreover, markers of DNA damage and impaired nuclear integrity (seen in islet senescence) (*32*) were enriched in male mutant islets from the mixed, but not C57, background (**Fig. 4D-E**). No islet senescence signatures are seen in female Het islets of either background (**Supp Fig. 3A-B**).

RNASeq analyses shows improvement of senescence signatures in C57 MafA$^{S64F/+}$ males compared to mixed background MafA$^{S64F/+}$ males.

We next took an unbiased approach to further evaluate the molecular differences between the male MafA^{WT} and MafA$^{S64F/+}$ mice of mixed and C57 genetic backgrounds showing dysglycemia and its genetic rescue, respectively. We isolated islets from males of each background at 5

weeks of age (age of phenotype onset); islet recovery was markedly reduced in MafA$^{S64F/+}$ mice of a mixed background as we had seen previously (*18*), but recovery was significantly improved on the C57 background (**Fig. 5A**). We performed bulk RNASeq to assess dominant gene expression patterns between these groups. Unbiased clustering identified that the molecular signatures between MafA^{WT} and MafA$^{S64F/+}$ males on a C57 background were more similar than between MafA^{WT} and MafA^{S64F} male islets on a mixed background (**Fig. 5B**). Differentially expressed genes were then evaluated: MafA$^{S64F/+}$ mice of C57 background had 2,097 differentially expressed genes (DEGs) (616 up and 1481 down) compared to male WT islets on this background, while MafA$^{S64F/+}$ mice of mixed background had 3,366 DEGs (1505 up and 1861 down) (**Fig. 5C**). There were also 386 upregulated and 621 downregulated DEGs that were similarly regulated between the backgrounds. We evaluated senescence-associated gene expression and found them to be enriched in the MafA$^{S64F/+}$ males on a mixed, but less on the C57, background (**Fig. 5D**).

Unbiased RNASeq analysis also revealed expression differences of genes regulating β-cell identity and circadian rhythm

We decided to evaluate DEGs of MafA$^{S64F/+}$ males that were unique to each genetic background (i.e. 855 downregulated and 228 upregulated in the C57 MafA$^{S64F/+}$ background males, vs. 1238 downregulated and 1114 upregulated in the MafA$^{S64F/+}$ mixed background males) (**Fig. 5C**). Gene Ontology analysis of the DEGs identified in MafA$^{S64F/+}$ males on both C57 and mixed background by bulk RNAseq identified upregulated pathways involved in pancreatic exocrine secretion, protein digestion and absorption, calcium signaling pathways (**Fig. 6A**), as we had seen previously (*18*), with greater significance of these pathways in the mixed background. Pathways that were downregulated in the mixed background included neuroactive ligand-receptor interactions and circadian entrainment. Downregulated pathways on the C57 background included nuclear receptors in lipid metabolism and retinol metabolism.

We then performed STRING analysis (*33*) of the DEGs unique to each genetic background to further evaluate function protein association networks. Networks significantly changed in MafA$^{S64F/+}$ mixed background males was protein digestion, calcium signaling, neuroactive ligands (such as Sst, Npy), and circadian entrainment (**Fig 6B**), suggesting that disturbances in islet β-cell circadian entrainment contributes to the dysglycemia in MafA$^{S64F/+}$ mixed background males. These results suggest that despite the unique DEGs and pathways

enriched in each background, there are common pathways similarly changed (albeit at lower significance in the C57 background) between the two backgrounds.

Overlay of differentially expressed genes unique only to C57 MafA$^{S64F/+}$ vs. Mixed MafA$^{S64F/+}$ males with MafA CUT&RUN peaks identifies influence of circadian entrainment.

We then questioned whether the DEGs uniquely identified in each background were a target of the MafA transcription factor. We performed CUT&RUN for endogenous MafA in Min6 cells, and peaks were annotated by nearest gene (n=11,403 genes identified) (**Fig. 7A**). We then overlaid these annotated peaks with the DEGs uniquely identified in MafA$^{S64F/+}$ males of each genetic background (**Fig. 7A**). This analysis yielded 250 DEGs which could be direct targets of MafA in the C57 background, which included factors in the prosurvival Bcl2 family (ie. Bcl2l14), Slit/Robo signaling (Robo3), and retinoic acid signaling (e.g RAR α/β). Similar analysis yielded 1210 potential targets in MafA$^{S64F/+}$ male islets on a mixed background. These included genes associated with β-cell identity and islet hormones such as Ucn3, Gcg, Sst, Cck, Gast; islet enriched transcription factors and receptors such as Glis1, Glp1r, Nkx6.2, Nkx6.3, Onecut1 and Smarca1; and circadian entrainment Cry2, Per1, Per2, Rora, Dbp, Bhlhe40/Dec1, Nr1d1 (Rev-erba), Nr1d2 (Rev-erb) (**Fig. 7A-B**).

Circadian entrainment of islet β-cells is essential for β-cell function (*34, 35*). Here, islet gene expression showed a generalized repression of the circadian regulators: repressors such as Cry2, Per1, Per2, Bhlhe40/Dec1, and activators like Rora and Dbp in the MafA$^{S64F/+}$ males of the mixed background. Expression heatmap analysis of circadian entrainment showed downregulation of critical regulators in our bulk RNAseq samples (**Fig. 6C-D**). Interestingly, the core circadian activators Bmal and Clock were unchanged between genotypes and genetic background, suggesting that the genetic-background related dysglycemia of MafA$^{S64F/+}$ males is influenced by cellular aging and regulators of circadian entrainment.

DISCUSSION

MafA is a critical β-cell maturity factor (reviewed in (*28*)), and prior work has highlighted the therapeutic potential of strategies that can maintain MAFA levels in β-cells (*6*). In vitro analysis demonstrated that a mutation substituting a serine residue to phenylalanine at position 64 (i.e. Ser64Phe, or S64F) and impairs a key priming phosphorylation event at position Ser65 in MAFA, which profoundly increases the stability of the MAFA by impairing posttranslational modifications necessary for ubiquitin-mediated degradation (*17*). Since this original report, a second MafA missense mutation in the transactivation domain have been identified in which carriers develop dysglycemia and also predicted to promote MafA protein stability (*36*), confirming the unexpected pathogenicity of stabilizing MafA mutations. We then generated a mouse model harboring the S64F mutation in the endogenous *Mafa* gene which recapitulated the heterogenous responses seen in patients (*18*), providing surprising insights into the impact of elevating MafA levels *in vivo*. Moreover, our efforts in this report backcrossing these mice on the C57 background revealed that genetic background also influences to the susceptibility of the male (moreso than female) phenotype. Males $MafA^{S64F/+}$ mice on a mixed genetic background of C57/Bl6J and SJL show overt diabetes and impaired GSIS by 5 weeks of age, while those on a C57/Bl6J background maintain intact insulin secretion and euglycemia. Comparing these mutant lines reveal differences in β-cell senescence and reduced proportion of the underphosphorylated $MafA^{S64F}$ species in the C57 background. Unbiased RNAseq analysis uncovered a genetic background-specific dysregulation of circadian regulators, identifying a novel link between β-cell maturity driver like MafA, cellular aging, and circadian entrainment.

Circadian rhythm is critical in general metabolism and specifically pancreatic β-cell function and insulin secretion. The core clock transcription factors Clock and Bmal1 are essential for dynamic insulin secretion synchronized with the oscillatory expression of genes encoding secretory machinery and factors regulating insulin release, such as Pdx1 (*34, 35*). Periodicity of these core factors are regulated by autoregulatory loops driven by post-translational modifications such as ubiquitination and phosphorylation, akin to the Maf transcription factors (*28*). Ubiquitination by ubiquitin ligases such as FBXL3/21 and TRCP1/2 also regulates the periodicity of clock repressors of such as Cry1/2 and Per1/2, respectively (*37-40*). Ultimately, these processes link transcriptional output (such as *Insulin*), circadian rhythmicity and cellular physiology. Future efforts are needed to study the impact of $MafA^{WT}$ and $MafA^{S64F}$ on synchronized mice and cell systems on assess the integrity of the β-cell clock mechanisms. Forward genetic screens to identify other potential MafA co-regulators (such as

ubiquitin ligases) that can mediate these effects across these genetic backgrounds are also warranted.

The coexistence of dysregulated circadian entrainment and accelerated senescence is interesting, and it is unclear whether these processes occur in parallel or along a common pathway to disturb insulin secretion. Intriguingly, the core clock repressors identified here do not have MARE (MAF consensus) binding sites nor are they recognized to bind MAFA/B in human islets (Islet regulome (*41*)). This suggests that while MAFA may not directly bind to these genes but rather is a component of a scaffolding complex for other regulators to cooperatively bind. Directed evaluation of β-cell senescence in models of disturbed circadian regulation would be fruitful, as would the evaluation of circadian dysregulation on other well-studied models of dysglycemia showing β-cell senescence, such as the NOD model (*31*) and in models of insulin-resistance (*30*).

Nevertheless, our work here demonstrates the combinatorial impact of genetic background and biologic sex on molecular and functional β-cell responses to produce heterogenous responses (i.e. cellular senescence driving dysfunction vs. hypoglycemia). Our data strongly suggest that these different responses to $MafA^{S64F}$ may be mediated by changes in the fundamental circadian regulators and facilitate our ultimate goal to develop strategies to safely optimize β-cell function in people with diabetes.

Acknowledgements. This research was performed using resources and/or funding provided by NIH grants to JC (K08 DK132507), RS (R01 DK090570), and by the Vanderbilt Diabetes Research and Training Center (DK20593). JC is also supported by a Burroughs Wellcome Fund Career Award for Medical Scientists and institutional funds from VUMC. The authors thank the members of Rafael Arrojo e Drigo Lab (Vanderbilt University) and the Joseph Bass Lab (Northwestern University) for critical discussion.

Duality of Interest. No potential conflicts of interest relevant to this article were reported.

Author Contributions.

ZL, DL, MM, MAM, RS, and JC designed the study.

ZL, DL, MM, JL, MG, GR, JPC, and JC performed experiments.

ZL, DL, JPC, and JC performed bioinformatic analysis.

ZL, DL, MM, JL, MG, GR, MAM, JPC, RS, and JC analyzed data.

DL, MM, and JC wrote the manuscript.

ZL and DL are co–first authors due to their contributions in most of the experimental studies.

MAIN FIGURE LEGENDS

Figure 1. Glucose tolerance is largely unaffected in C57 MafA$^{S64F/+}$ males, while those on a Mixed background manifest frank diabetes and impaired insulin secretion

A. Fasted male animals underwent intraperitoneal glucose tolerance tests at various time points as indicated. Male MafA$^{S64F/+}$ heterozygous (termed "Het") mice on a C57 background had no changes to glucose tolerance through adulthood compared to MafA$^{+/+}$ (termed "WT") male littermates

B. Fasted male animals underwent intraperitoneal glucose tolerance tests (GTT) at time points indicated. Het males on a Mixed background had impaired glucose tolerance by 5 weeks of age which then progressed to overt diabetes by 7 weeks of age.

C-D. Stimulated in vivo C-peptide (C) and insulin (D) measurements showed reduction in Het males at 5.5 weeks of age on a Mixed background. Two-tailed Student t test; *$p < 0.05$; **$p < 0.01$

E. Stimulated in vivo C-peptide measurements showed no significant changes between WT and Het males at 5.5 weeks of age on a C57 background

Figure 2. Islet endocrine populations are largely unchanged, however, expression of critical islet factors and known MafA targets are altered in MafA$^{S64F/+}$ islets despite MafA^{S64F} binding to the *Insulin* enhancer being similar to MafA^{WT}.

A-B. Immunostaining showing intact islet hormone^{+} cells and distribution between C57 (A) and Mixed background (B) males at 5 weeks of age.

C-D. qPCR of critical islet factors and known MAFA targets are altered in C57 vs. Het male mice. *$p < 0.05$; **$p < 0.01$; ***$p < 0.001$

E. Gel shift assay of HeLa nuclear extract (NE) produced MAFA^{WT} and mutant MAFA^{S64F} bound to *INS* enhancer (known MAFA target), showing similar binding affinity. Specificity of MAFA binding showed by super shift (SS) with MafA antibody.

Figure 3. Phosphorylated MafA species are more preserved in islets of MafA$^{S64F/+}$ C57 male islets compared to those from a mixed background

A,C. qPCR for *MafA*, *MafB*, and *Ins1* differs in Het male islets of mixed background (A) but intact in C57 Het males (C). *$p < 0.05$.

B, D. Immunostaining for MafA show poor detection in Mixed background male Het islets (B) but intact MafA in C57 male Het islets (D). Islets from MafA$^{\Delta\beta}$ included as a negative control

E. Left lanes, Western blotting on MIN6 nuclear extract transfected to express either $MAFA^{WT}$ or $MAFA^{S64F}$ shows faster migration in mutant MAFA due to impaired posttranslational modification by phosphorylation. Right lanes, Isolated mouse islets from each genotype and background showed detectable levels of phosphorylated (active) MAFA in C57 background, but relative uniformity of MAFA species with impaired phosphorylation in the Mixed background.

F. Quantification of Western blotting bands by Line scan analysis shows greater proportion of phosphorylated MafA species (gray) in Het male islets from the C57 background compared to the Mixed background.

Figure 4. Islet senescence is abrogated in $MafA^{S64F/+}$ C57 male islets.

A. Senescence associated beta gal staining (SA-β-gal) is enriched in male Het islets from the Mixed background, and qPCR of senescence signature genes are significantly altered in C57 islets at 5 weeks of age. *$p < 0.05$

B. SA-β-gal staining not detectable in male Het islets from the C57 background, and qPCR of senescence signature genes are unchanged in C57 islets at 5 weeks of age. *$p < 0.05$

C. Top, RNAScope for *Cdkn1a* encoding p21 shows enrichment in Het islets on a mixed background in β-cells. Bottom, Quantification of *Cdkn1a*$^+$Ins$^+$ cells. *$p < 0.05$

D-E. Immunostaining of senescence markers show enrichment of 53BP1 and relative loss of nuclear LaminB1 in the mixed (D), but not C57 (E), background.

Figure 5. RNASeq shows improvement of global senescence signatures in islets of $MafA^{S64F/+}$ C57 male islets compared to those of a mixed background

A. Representative images of male islet isolation yield from each genotype and genetic background, with markedly paler islets and poorer yields in Het males on a mixed background

B. Unbiased hierarchical clustering showed congruent organization within genotypes and genetic background

C. Venn diagram illustrates the total number of RNA-seq-identified DEGs up- or down-regulated between 5-week-old WT and Het male islets of each background

D. Heatmaps showing aging/senescence enrichment in Mixed, but not C57, Het male islets.

Figure 6. Deregulation of circadian rhythm pathway in $MafA^{S64F/+}$ islets on a mixed, but not C57, background

A. Gene Ontology (GO): molecular function analysis ($p < 0.05$) of the genes uniquely up- or down-regulated in each genetic background in male Het islets.

B. STRING analysis identified enrichment of pathways from DEG's identified from bulk RNASeq analysis, including proteoglycan and protein digestion, calcium signaling, neuroactive ligands and circadian rhythm.

Figure 7. Overlay of MAFA Cut&Run peaks with differentially expressed genes unique only to C57 MafA$^{S64F/+}$ or Mixed MafA$^{S64F/+}$ males

A. DEGs identified uniquely in Male Het islets from a mixed background (1238 + 1114 = 2352 genes) versus those uniquely from a C57 background (228 + 855 = 1083 genes) were then overlayed with peaks identified by endogenous MafA CUT&RUN in mouse MIN6 cells (n=11403 peaks). Of these, 250 genes uniquely enriched in a C57 background overlapped with a MafA CUT&RUN peak, while 1210 were uniquely enriched in a Mixed background overlapped with a MafA CUT&RUN peak.

B. UCSC Genome Browser tracks showing genomic regions associated with endogenous MafA CUT&RUN peaks near known targets Ins1, Ins2, and Pdx1, and candidate gene Per1, Per2, and Cry2; MafA CUT&RUN enriched peaks are highlighted in dashed boxes, and regulated genes are depicted below IgG control tracks.

C. Heatmap of differentially expressed circadian rhythm genes from bulk RNASeq analysis

D. TPM counts of circadian rhythm genes showing downregulation in Het male islets of a Mixed, but not C57 background only

SUPPLEMENTAL FIGURE LEGENDS

Supplemental Figure 1. Hypoglycemia of MafA$^{S64F/+}$ females are similar between C57 and Mixed backgrounds

A. Fasted female animals underwent intraperitoneal glucose tolerance tests at various time points as indicated. Female MafA$^{S64F/+}$ heterozygous (termed "Het") mice on a C57 background showed persistent, mild hypoglycemia through postnatal life. *$p < 0.05$; **$p < 0.01$; ***$p < 0.001$.

B. Fasted female animals underwent intraperitoneal glucose tolerance tests at time points as indicated. Female Het mice on a mixed background showed persistent, mild hypoglycemia through postnatal life. *$p < 0.05$; **$p < 0.01$; ***$p < 0.001$.

C-D. Stimulated in vivo C-peptide (D) and insulin (E) measurements showed no significant changes at 5.5 weeks of age on a Mixed background.

E. Stimulated in vivo C-peptide measurements showed increased secretion in Het females at 5.5 weeks of age on a C57 background. *$p < 0.05$.

Supplemental Figure 2. Mixed background male and female MafA$^{S64F/+}$ show hypoglycemia while nursing, extended wean does not impact hyperglycemia in Male Hets, and weight gain and insulin tolerance are similar between the genetic backgrounds

A. Random blood glucose monitoring at 2-3 weeks of age while nursing shows similar mild, transient hypoglycemia in Male and Female Het mice on a mixed background. *$p < 0.05$; **$p < 0.01$

B. Random glucose level of suckling male Het mice on a mixed background at 5 weeks of age during an extended wean still reveals hyperglycemia, suggesting that the weaning process does not precipitate dysglycemia. *$p < 0.05$; **$p < 0.01$

C-D. Weight gain as a proxy for overall health across genotypes, biologic sex, and age does not appear significantly altered between groups

E. Insulin tolerance testing showing similar peripheral insulin sensitivity in male and female WT and Het mice on a mixed background.

Supplemental Figure 3. Islet senescence signatures are not seen in female Het islets of either background

A-B. qPCR of senescence signature genes are unchanged in Mixed (A) and C57 (B) background female MafA$^{S64F/+}$ islets at 5 weeks of age.

REFERENCES

1. C. Aguayo-Mazzucato, A. Koh *et al.*, MafA expression enhances glucose-responsive insulin secretion in neonatal rat β cells. *Diabetologia* **54**, 583-593 (2011).
2. L. Wang, Y. Huang *et al.*, Differentiation of iPSCs into insulin-producing cells via adenoviral transfection of PDX-1, NeuroD1 and MafA. *Diabetes Res Clin Pract* **104**, 383-392 (2014).
3. A. Jeyagaran, M. Urbanczyk *et al.*, Forward programming of hiPSCs towards beta-like cells using Ngn3, Pdx1, and MafA. *Sci Rep* **14**, 13608 (2024).
4. T. A. Matsuoka, H. Kaneto *et al.*, Preserving Mafa expression in diabetic islet beta-cells improves glycemic control in vivo. *J Biol Chem* **290**, 7647-7657 (2015).
5. H. Kaneto, T. A. Matsuoka *et al.*, A crucial role of MafA as a novel therapeutic target for diabetes. *J Biol Chem* **280**, 15047-15052 (2005).
6. I. El Khattabi, A. Sharma, Proper activation of MafA is required for optimal differentiation and maturation of pancreatic beta-cells. *Best Pract Res Clin Endocrinol Metab* **29**, 821-831 (2015).
7. J. Liang, M. Chirikjian *et al.*, MafA Regulation in beta-Cells: From Transcriptional to Post-Translational Mechanisms. *Biomolecules* **12**, (2022).
8. I. Artner, Y. Hang *et al.*, MafA and MafB regulate genes critical to β cells in a unique temporal manner. *Diabetes* **59**, 2530-2539 (2010).
9. H. A. Cyphert, E. M. Walker *et al.*, Examining how the MAFB transcription factor affects islet β cell function postnatally. *Diabetes* **68**, 337-348 (2019).
10. Y. Hang, T. Yamamoto *et al.*, The MafA transcription factor becomes essential to islet β cells soon after birth. *Diabetes* **63**, 1994-2005 (2014).
11. C. Zhang, T. Moriguchi *et al.*, MafA is a key regulator of glucose-stimulated insulin secretion. *Mol Cell Biol* **25**, 4969-4976 (2005).
12. C. Luan, Y. Ye *et al.*, The calcium channel subunit gamma-4 is regulated by MafA and necessary for pancreatic β cell specification. *Commun Biol* **2**, 106 (2019).
13. J. Cha, X. Tong *et al.*, Species-specific roles for the MAFA and MAFB transcription factors in regulating islet beta cell identity. *JCI Insight* **8**, (2023).
14. S. Guo, C. Dai *et al.*, Inactivation of specific β cell transcription factors in type 2 diabetes. *J Clin Invest* **123**, 3305-3316 (2013).
15. L. R. Cataldo, T. Singh *et al.*, MAFA and MAFB regulate exocytosis-related genes in human beta-cells. *Acta Physiol (Oxf)* **234**, e13761 (2022).
16. A. Bonnefond, R. Unnikrishnan *et al.*, Monogenic diabetes. *Nat Rev Dis Primers* **9**, 12 (2023).
17. D. Iacovazzo, S. E. Flanagan *et al.*, MAFA missense mutation causes familial insulinomatosis and diabetes mellitus. *Proc Natl Acad Sci U S A* **115**, 1027-1032 (2018).
18. E. M. Walker, J. Cha *et al.*, Sex-biased islet beta cell dysfunction is caused by the MODY MAFA S64F variant by inducing premature aging and senescence in males. *Cell Rep* **37**, 109813 (2021).
19. M. Gannon, R. N. Kulkarni *et al.*, Sex differences underlying pancreatic islet biology and its dysfunction. *Mol Metab* **15**, 82-91 (2018).
20. M. P. Keller, M. E. Rabaglia *et al.*, Gene loci associated with insulin secretion in islets from non-diabetic mice. *J Clin Invest* **129**, 4419-4432 (2019).
21. J. Cha, X. Tong *et al.*, Defining unique structural features in the MAFA and MAFB transcription factors that control Insulin gene activity. *J Biol Chem*, 107938 (2024).
22. P. Bankhead, M. B. Loughrey *et al.*, QuPath: Open source software for digital pathology image analysis. *Sci Rep* **7**, 16878 (2017).

23. U. Schmidt, Weigert, M., Broaddus, C., Myers, G., Cell detection with star-convex polygons. *International Conference on Medical Image Computing and Computer-Assisted Intervention (MICCAI)*, (2018).
24. C. Benner, T. van der Meulen *et al.*, The transcriptional landscape of mouse beta cells compared to human beta cells reveals notable species differences in long non-coding RNA and protein-coding gene expression. *BMC Genomics* **15**, 620 (2014).
25. M. P. Meers, T. D. Bryson *et al.*, Improved CUT&RUN chromatin profiling tools. *Elife* **8**, (2019).
26. A. L. Lin, J.P. Cartailler, in *peakScout – a user-friendly and reversible peak-to-gene translator for genomic peak calling results: https://github.com/vandydata/peakScout*. (2025).
27. Y. Song, in *ggcoverage - Visualize and annotate omics coverage with ggplot2: https://showteeth.github.io/ggcoverage/*. (2025).
28. Y. Hang, R. Stein, MafA and MafB activity in pancreatic β cells. *Trends Endocrinol Metab* **22**, 364-373 (2011).
29. J. S. Harmon, R. Stein, R. P. Robertson, Oxidative stress-mediated, post-translational loss of MafA protein as a contributing mechanism to loss of insulin gene expression in glucotoxic beta cells. *J Biol Chem* **280**, 11107-11113 (2005).
30. C. Aguayo-Mazzucato, J. Andle *et al.*, Acceleration of β cell aging determines diabetes and senolysis improves disease outcomes. *Cell Metab* **30**, 129-142 e124 (2019).
31. P. J. Thompson, A. Shah *et al.*, Targeted elimination of senescent β cells prevents type 1 diabetes. *Cell Metab* **29**, 1045-1060 e1010 (2019).
32. J. Cha, C. Aguayo-Mazzucato, P. J. Thompson, Pancreatic beta-cell senescence in diabetes: mechanisms, markers and therapies. *Front Endocrinol (Lausanne)* **14**, 1212716 (2023).
33. D. Szklarczyk, R. Kirsch *et al.*, The STRING database in 2023: protein-protein association networks and functional enrichment analyses for any sequenced genome of interest. *Nucleic Acids Res* **51**, D638-D646 (2023).
34. B. J. Weidemann, B. Marcheva *et al.*, Repression of latent NF-kappaB enhancers by PDX1 regulates beta cell functional heterogeneity. *Cell Metab* **36**, 90-102 e107 (2024).
35. M. Perelis, B. Marcheva *et al.*, Pancreatic beta cell enhancers regulate rhythmic transcription of genes controlling insulin secretion. *Science* **350**, aac4250 (2015).
36. C. Fottner, S. Sollfrank *et al.*, Second MAFA Variant Causing a Phosphorylation Defect in the Transactivation Domain and Familial Insulinomatosis. *Cancers (Basel)* **14**, (2022).
37. K. Stojkovic, S. S. Wing, N. Cermakian, A central role for ubiquitination within a circadian clock protein modification code. *Front Mol Neurosci* **7**, 69 (2014).
38. A. Hirano, K. Yumimoto *et al.*, FBXL21 regulates oscillation of the circadian clock through ubiquitination and stabilization of cryptochromes. *Cell* **152**, 1106-1118 (2013).
39. S. H. Yoo, J. A. Mohawk *et al.*, Competing E3 ubiquitin ligases govern circadian periodicity by degradation of CRY in nucleus and cytoplasm. *Cell* **152**, 1091-1105 (2013).
40. K. Ohsaki, K. Oishi *et al.*, The role of beta-TrCP1 and beta-TrCP2 in circadian rhythm generation by mediating degradation of clock protein PER2. *J Biochem* **144**, 609-618 (2008).
41. L. Pasquali, K. J. Gaulton *et al.*, Pancreatic islet enhancer clusters enriched in type 2 diabetes risk-associated variants. *Nat Genet* **46**, 136-143 (2014).

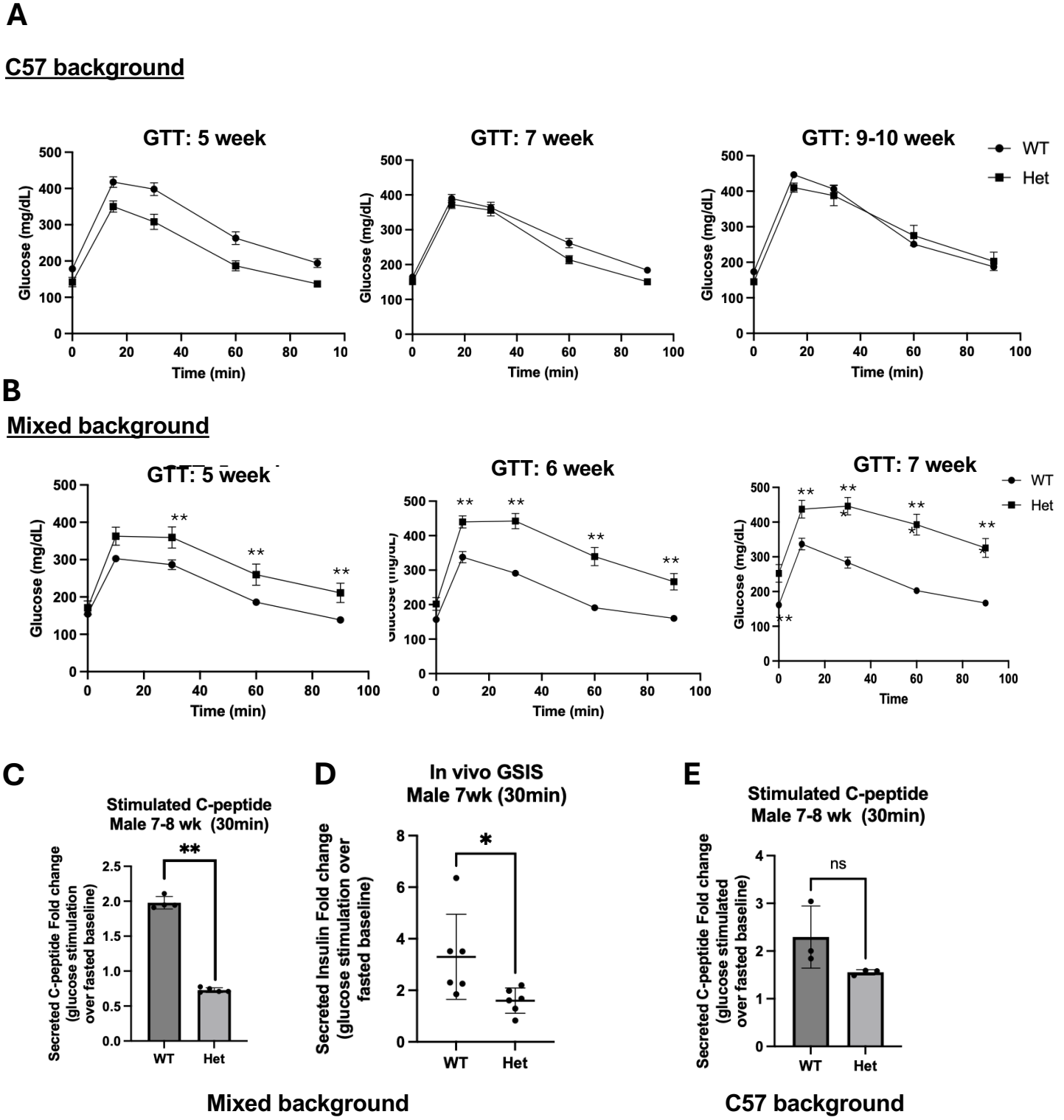

Main figure 1

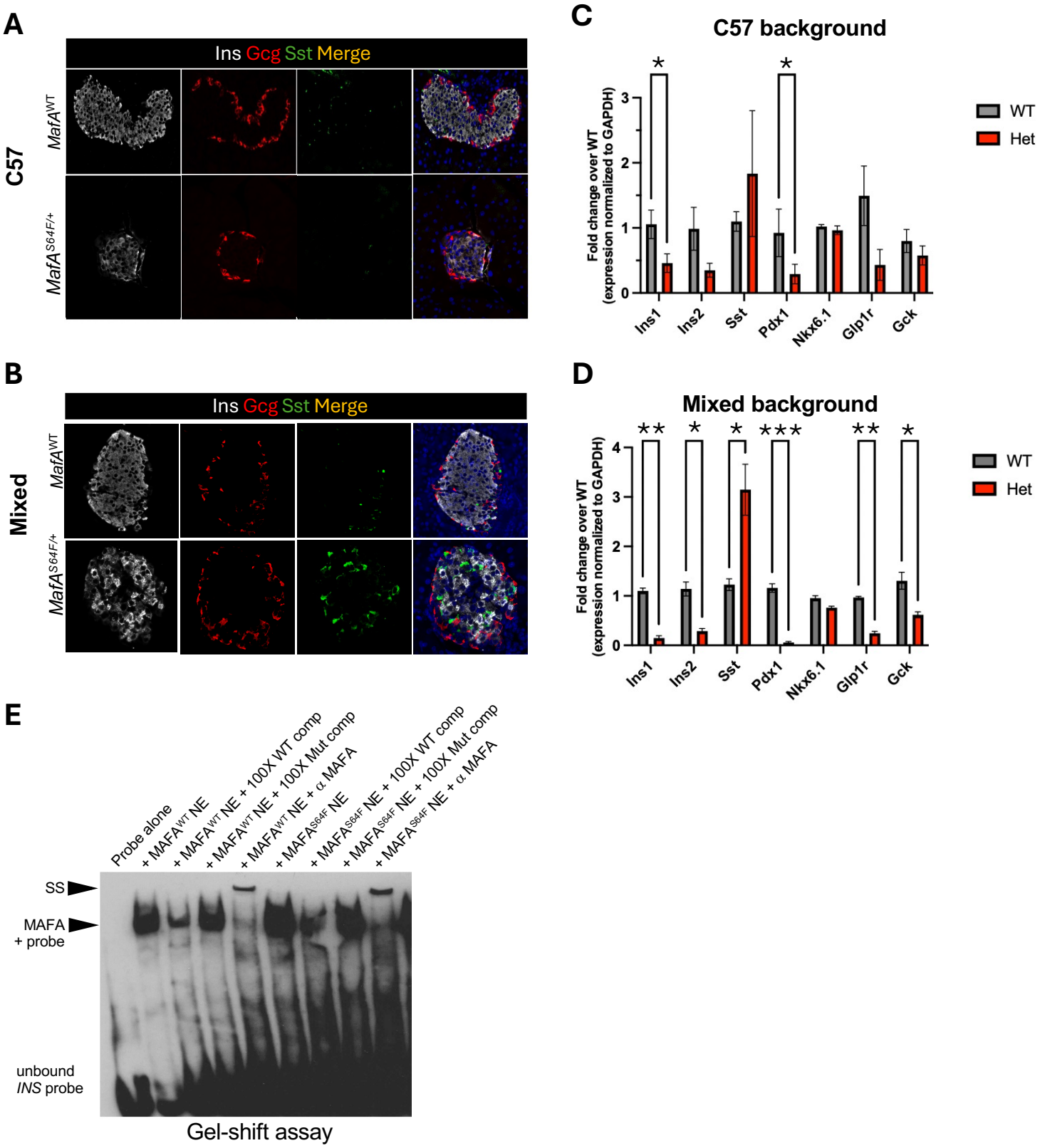

Main figure 2

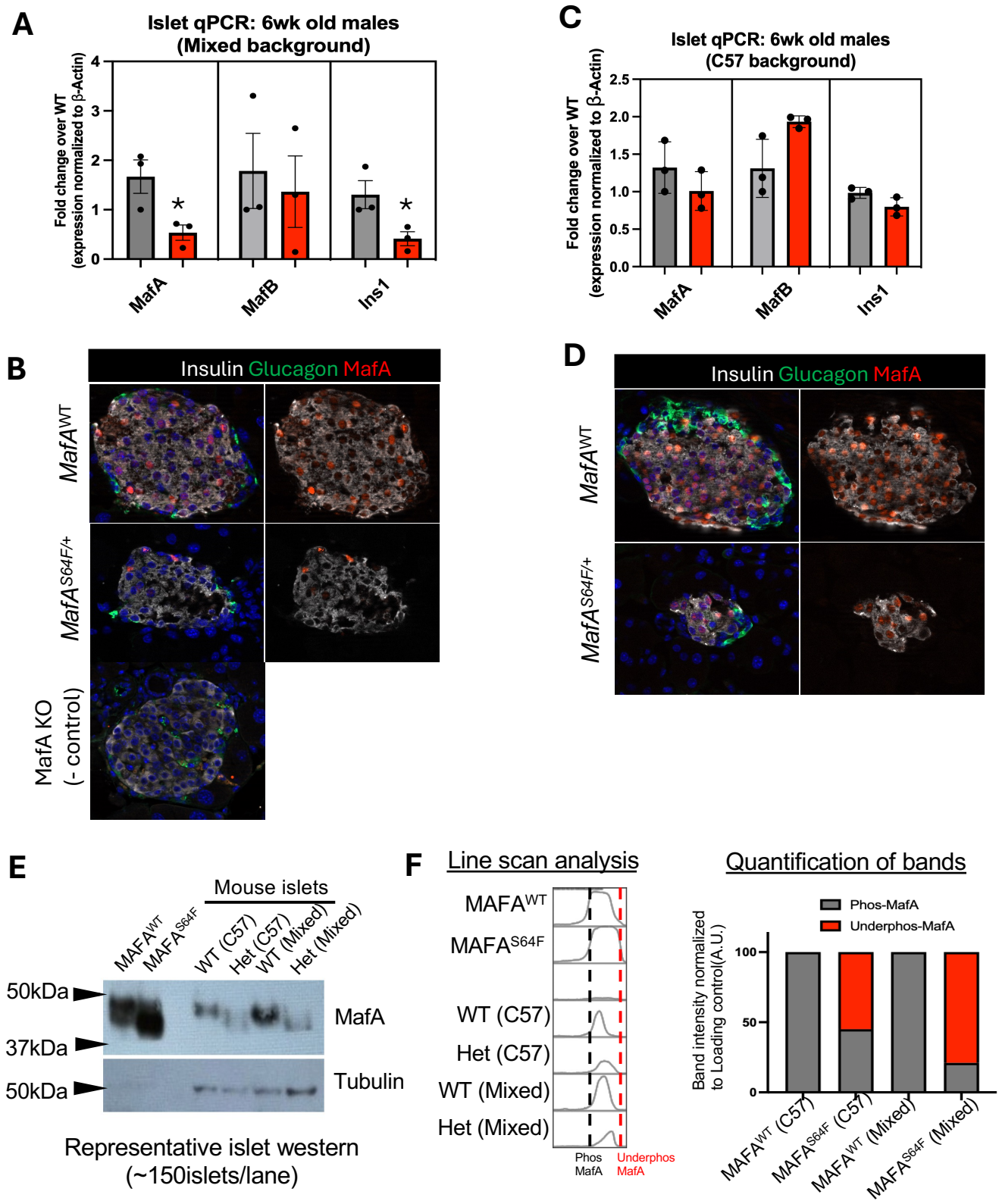

Main figure 3

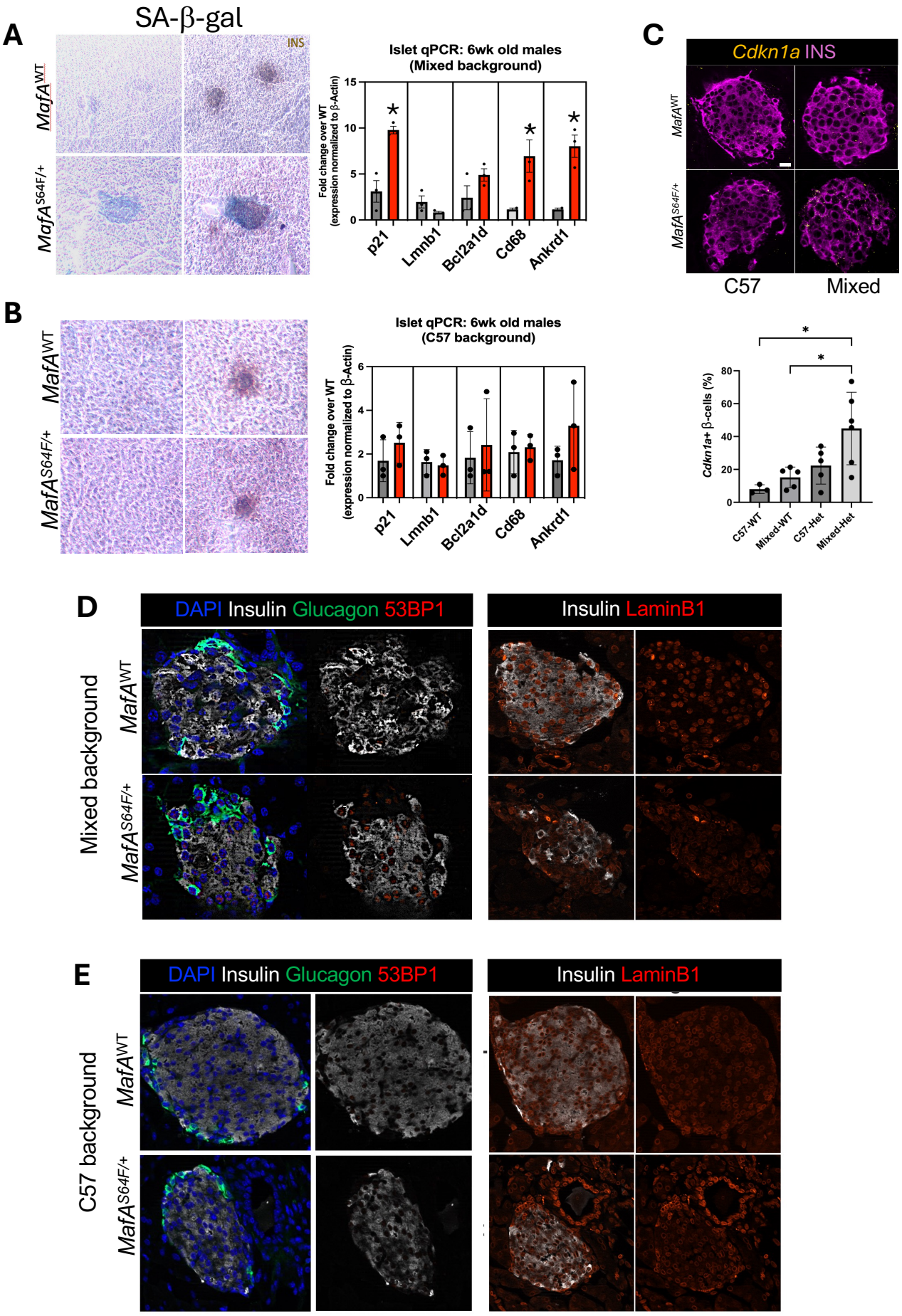

Main figure 4

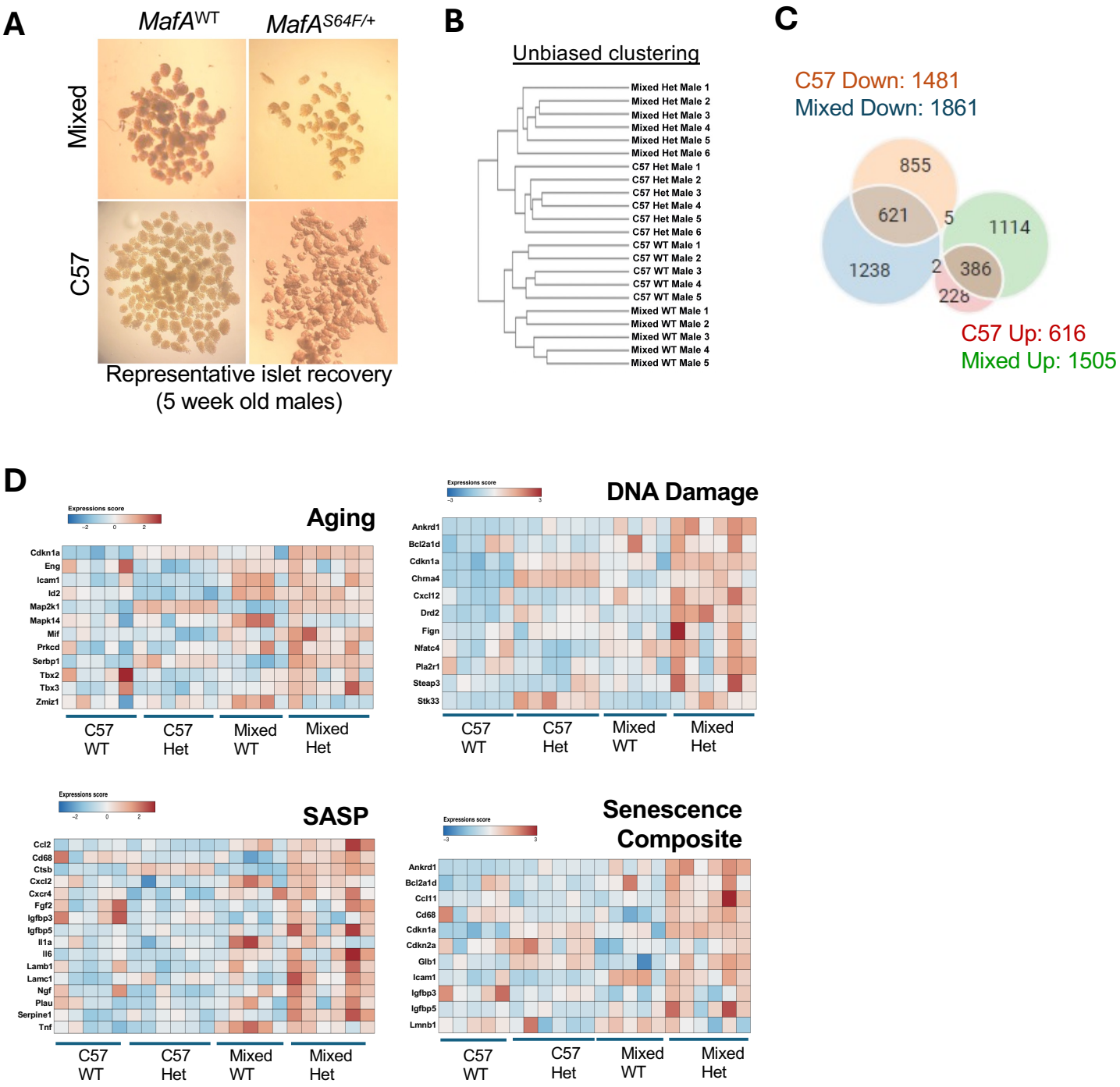

Main figure 5

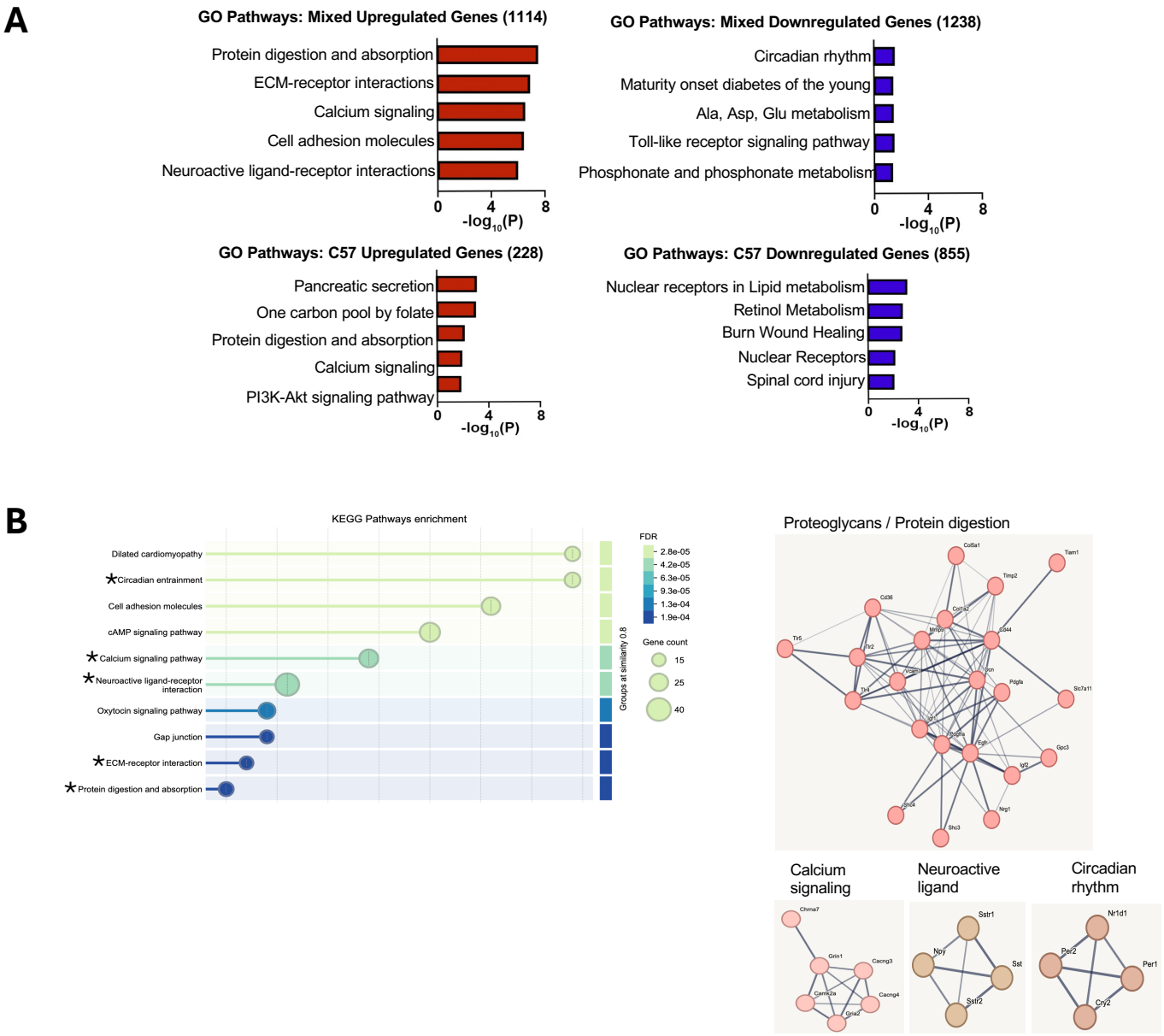

Main figure 6

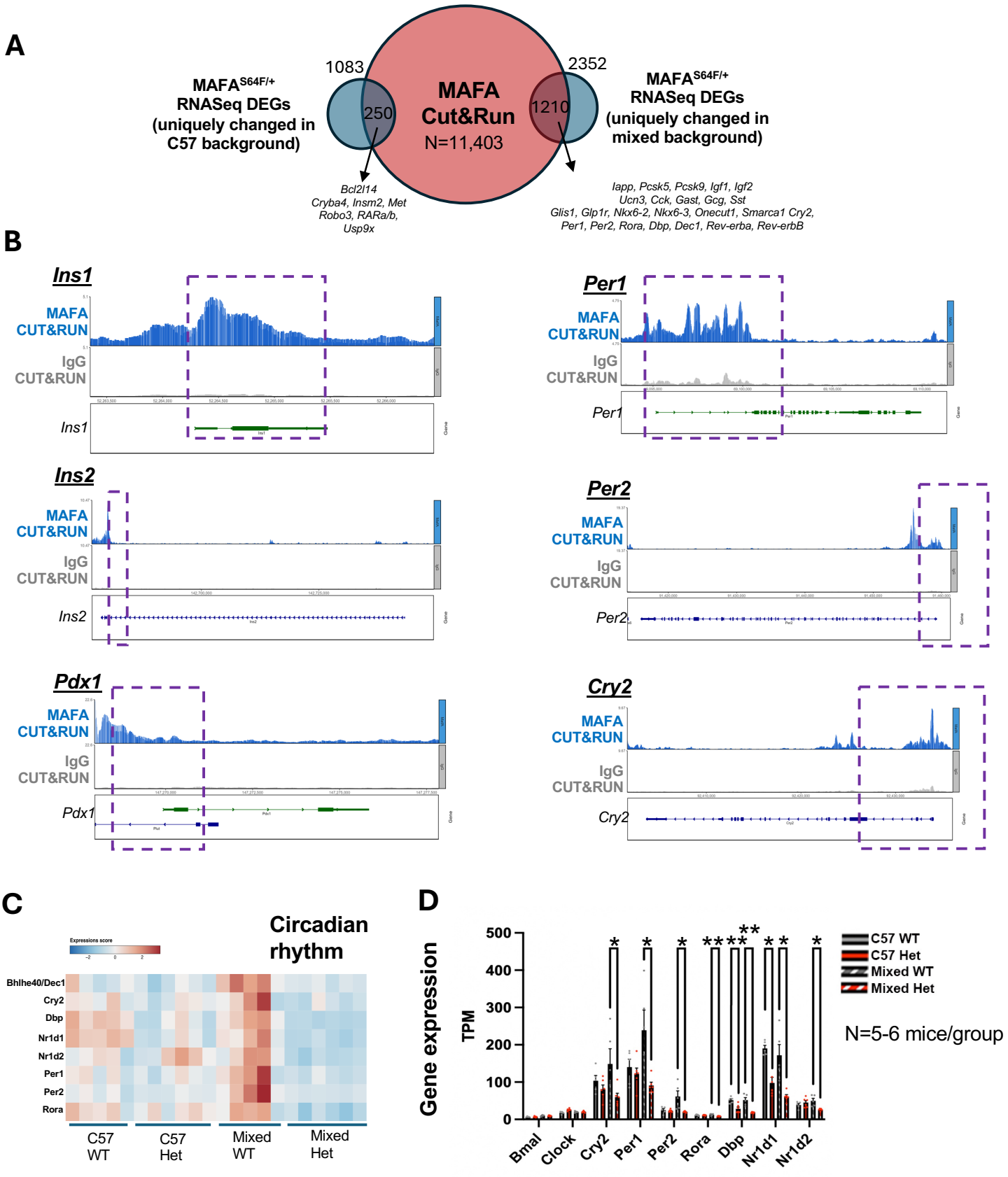

Main figure 7